Journal of Power Sources 186 (2009) 244–251

Contents lists available at ScienceDirect

Journal of Power Sources

journal homepage: www.elsevier.com/locate/jpowsour

Effect of a reducing agent for silver on the electrochemical activity of an $Ag/Ba_{0.5}Sr_{0.5}Co_{0.8}Fe_{0.2}O_{3-\delta}$ electrode prepared by electroless deposition technique

Wei Zhou, Ran Ran, Rui Cai, Zongping Shao*, Wanqin Jin, Nanping Xu

State Key Laboratory of Materials-Oriented Chemical Engineering, College of Chemistry & Chemical Engineering, Nanjing University of Technology, No. 5 Xin Mofan Road, Nanjing 210009, PR China

ARTICLE INFO

Article history:
Received 30 August 2008
Received in revised form 14 October 2008
Accepted 15 October 2008
Available online 1 November 2008

Keywords:
$Ag/Ba_{0.5}Sr_{0.5}Co_{0.8}Fe_{0.2}O_{3-\delta}$
Cathode
Solid-oxide fuel cell
Electrochemical impedance
Electroless deposition

ABSTRACT

Silver-modified $Ba_{0.5}Sr_{0.5}Co_{0.8}Fe_{0.2}O_{3-\delta}$ (Ag/BSCF) electrodes were prepared using an electroless deposition technique. The morphology, microstructure and oxygen reduction reaction activity of the resulted Ag/BSCF electrodes were comparatively studied using Fourier transform infrared spectra, environmental scanning electron microscopy, temperature-programmed oxygen desorption, X-ray diffraction, and electrochemical impedance spectroscopy. An area-specific resistance as low as 0.038 $\Omega\,cm^2$ was achieved for N_2H_4-reduced Ag/BSCF cathode at 600 °C. Carbonates were detected over the BSCF surface during the reduction of silver, which deteriorated both the charge-transfer process and diffusion process of HCHO-reduced Ag/BSCF cathode for the oxygen electrochemical reduction reaction. An anode-supported single cell with an N_2H_4-reduced Ag/BSCF cathode showed a peak power of 826 mW cm^{-2} at 600 °C. In comparison, only 672 mW cm^{-2} was observed with the HCHO-reduced Ag/BSCF cathode.

1. Introduction

Advanced low-temperature (<600 °C) solid-oxide fuel cells (LTSOFCs) require highly functional cathode materials that can provide high ionic and electronic conductivity and high electrocatalytic activity in oxygen reduction reactions (ORR) to reduce polarization resistance at the cathode/electrolyte interface at reduced operating temperatures [1–5]. Recently, $Ba_{0.5}Sr_{0.5}Co_{0.8}Fe_{0.2}O_{3-\delta}$ (BSCF) perovskite oxide was successfully developed as a cathode for SOFCs operating at 600 °C [6,7]. However, low electronic conductivity makes BSCF unfavorable for applications below 600 °C. Considerable effort has been spent on attempts to increase the electrochemical activity of BSCF at lower temperatures, including the use of doping strategies and surface modifications with metals.

It is well known that the introduction of certain precious metals into the porous oxide electrode matrix can enhance electrocatalytic activity for ORR [8–15] due to the high activity of precious metals for oxygen reduction as well as the synergetic effect of precious metals and the oxide electrode. Silver is also known to perform a similar function [16–24]. Many techniques have been exploited for the synthesis of precious metal- or silver-modified oxide electrodes. Due to its lower cost, the idea of using silver as an electrode modifier has received considerable attention in the past several years. Very recently, an electroless deposition technique has been exploited to prepare silver-modified $Li_4Ti_5O_{12}$ composite electrodes for lithium-ion batteries [25] and silver-modified BSCF cathode for SOFCs [26,27]. These electrodes showed superior electrochemical performances as compared with those made from the traditional preparation methods, such as mechanical ball milling and impregnation-thermal decomposition. However, it was reported that reducing agents employed during the electroless deposition processes for electrodes designed for proton exchange membrane fuel cells (PEMFCs) could have a significant impact on the ORR activity [28]. In our previous study, we also observed that the electrochemical performance of the perovskite-type cathodes, such as BSCF and $La_{0.6}Sr_{0.4}Co_{0.2}Fe_{0.8}O_{3-\delta}$ (LSCF), was sensitive to the fabricating processes [29,30]. It is thus reasonable to expect that the reducing agents could also have an effect on the performance of silver-modified BSCF cathodes.

In order to further improve the electrochemical performance of BSCF-based electrodes, the reducing agent should be optimized. In this study, the reducing agent on the ORR catalytic activity of the silver-modified BSCF was investigated systematically. In particular, hydrazine (N_2H_4) and formaldehyde (HCHO) were adopted as reducing agents.

* Corresponding author. Tel.: +86 25 83172256; fax: +86 25 83365813.
E-mail address: shaozp@njut.edu.cn (Z. Shao).

0378-7753/$ – see front matter © 2008 Elsevier B.V. All rights reserved.
doi:10.1016/j.jpowsour.2008.10.055

2. Experimental

2.1. Preparation of the BSCF matrix

BSCF powders were synthesized by a combined EDTA–citrate complexing sol–gel process. The detailed procedure for this process has been reported in our prior publication Ref. [31]. In brief, required amounts of metal nitrates were prepared into a mixed solution followed by the addition of EDTA and citric acid at a pH of ~6, with the help of NH_4OH at a mole ratio of total metal ions:EDTA:citric acid of 1:1:2. The water was evaporated at 90 °C, resulting in transparent gels which were first pre-fired at 250 °C and then further calcined at 1000 °C for 5 h in air to produce the final products.

The prepared BSCF powder was dispersed in a premixed solution of glycerol, ethylene glycol and isopropyl alcohol to form a colloidal suspension through the use of a high-energy ball miller (Fritsch, Pulverisettle 6) at a rotational speed of 400 rpm for 0.5 h. The suspension was either symmetrically painted onto both surfaces of a dense SDC pellet with a diameter of ~13 mm and a thickness of ~0.8 mm, for the impedance test, or painted onto one side of SDC supported by SDC-NiO, for the fuel cell test. The thickness of the SDC thin film was ~30 μm. The BSCF matrix was then fired at 1000 °C for 2 h in air to make it adhere to the SDC electrolyte surface firmly.

2.2. Preparation of the Ag/BSCF composites

The silver precursor ($AgNO_3$ or $Ag(NH_3)_2^+$) solution (0.01 mol L^{-1}) was added in drops (using a suction pipette with an accuracy of ±0.01 mL) and soaked into the porous BSCF cathode layer, followed by heating at 80 °C to evaporate the water. During the preparation, the silver loading was controlled by adjusting the volume of the drops. The weight percentage of Ag to BSCF oxide was fixed at 3 wt.% unless other mentioned. After the impregnation of $AgNO_3$ into the BSCF matrix, the Ag^+ was reduced to Ag particles by HCHO or N_2H_4.

2.2.1. Electroless deposition by N_2H_4

When the desired silver loading was reached, the necessary amount of N_2H_4 solution at 0.01 mol L^{-1} was introduced as a reducing agent to induce the reduction of Ag^+ to Ag based on the equation:

$$4AgNO_3 + N_2H_4 = 4Ag + 4HNO_3 + N_2. \quad (1)$$

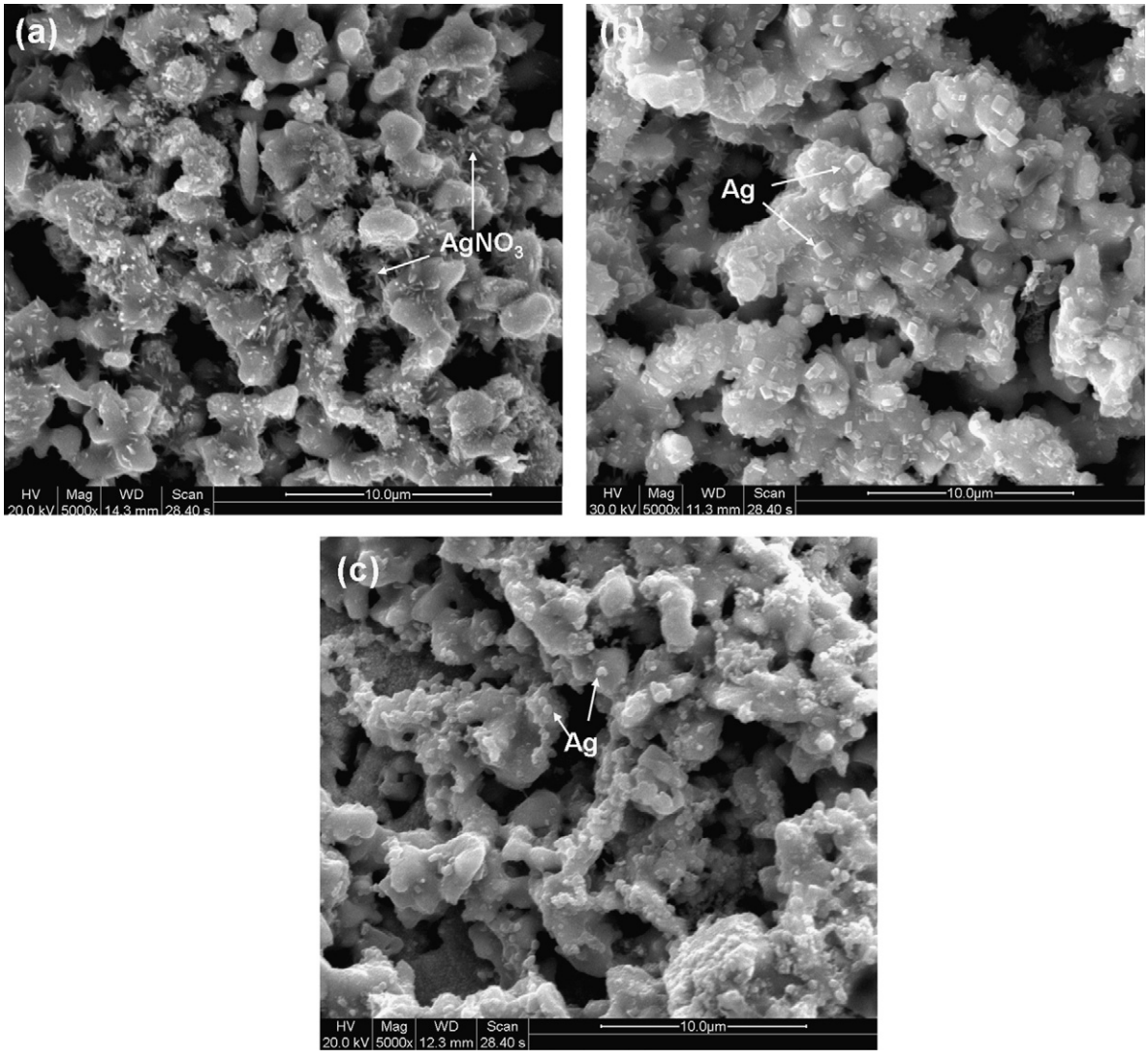

Fig. 1. SEM images of the $AgNO_3$ impregnated BSCF (a), and the as-prepared N_2H_4-reduced Ag/BSCF (b) and HCHO-reduced Ag/BSCF (c) cathodes.

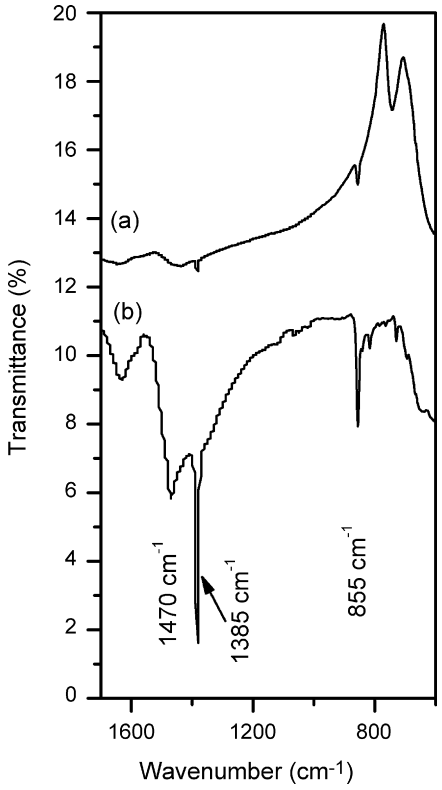

Fig. 2. FT-IR spectra of the as-prepared N_2H_4-reduced Ag/BSCF (a) and HCHO-reduced Ag/BSCF (b) composite powders.

Once the reaction was completed, the cell was heated at 80 °C over a hotplate, to evaporate the water from the electrode layer, and then fired at 850 °C for 30 min to form the N_2H_4-reduced Ag/BSCF cathode.

2.2.2. Electroless deposition by HCHO

Dilute $NH_3{\cdot}H_2O$ was titrated into the $AgNO_3$ solution at 0.01 mol L^{-1} until the white deposit disappeared to form the $Ag(NH_3)_2^+$ solution. The reactions can be described as follows:

$$Ag^+ + NH_3 \Leftrightarrow Ag(NH_3)^+, \quad (2)$$

$$Ag(NH_3)^+ + NH_3 \Leftrightarrow Ag(NH_3)_2^+. \quad (3)$$

The $Ag(NH_3)_2^+$ solution was introduced into the BSCF matrix, and the necessary amount of dilute HCHO was added as the reducing agent to induce the reduction of Ag^+ to Ag based on the equation:

$$2Ag(NH_3)_2^+ + HCHO + 2OH^- = 2Ag + HCOO^- + NH_4^+ + 3NH_3 + H_2O. \quad (4)$$

Once the reaction was completed, the cell was heated at 80 °C over a hotplate, to evaporate the water from the electrode layer, and then fired at 850 °C for 30 min to form the HCHO-reduced Ag/BSCF cathode.

2.3. Basic characterization

Phase compositions of the composite powders were analyzed by X-ray diffraction (XRD, Bruker D8 Advance) at room temperature. Fourier transform infrared spectroscopy (FT-IR, AVATAR-360) of the as-prepared powders was recorded from 4000 to 400 cm^{-1} using the KBr pellet method. The oxygen desorption properties of the composite powders were studied using an oxygen temperature-programmed desorption (O_2-TPD) technique. About 100 mg of the as-prepared powders were loaded in a quartz tube. The assembly was placed in a single-zone furnace equipped with a temperature controller. Argon was used as the carrier gas at a flow rate of 20 mL min^{-1} (STP). The temperature was increased from 50 to 950 °C at a rate of 10 °C min^{-1}. The effluent gases were monitored by a mass spectrometer (MS, Hiden, QIC-20). The microscopic features of the prepared electrodes were characterized using an environmental scanning electron microscopy (ESEM, QUANTA-2000).

2.4. Electrochemical performance test

An electrochemical cell with a four-terminal configuration was constructed. The *I–V* polarization was characterized using a Keithley 2420 source meter. Hydrogen, acting as a fuel, was fed into the anode chamber at a flow rate of 80 mL min^{-1} (STP); air, acting as the oxidant gas, was fed into the cathode chamber at a flow rate of 400 mL min^{-1} (STP). Gas flow rates were controlled with mass flow controllers, and a silver paste was used as the current collector.

The electrode performance was also investigated by ac impedance spectroscopy using an electrochemical workstation

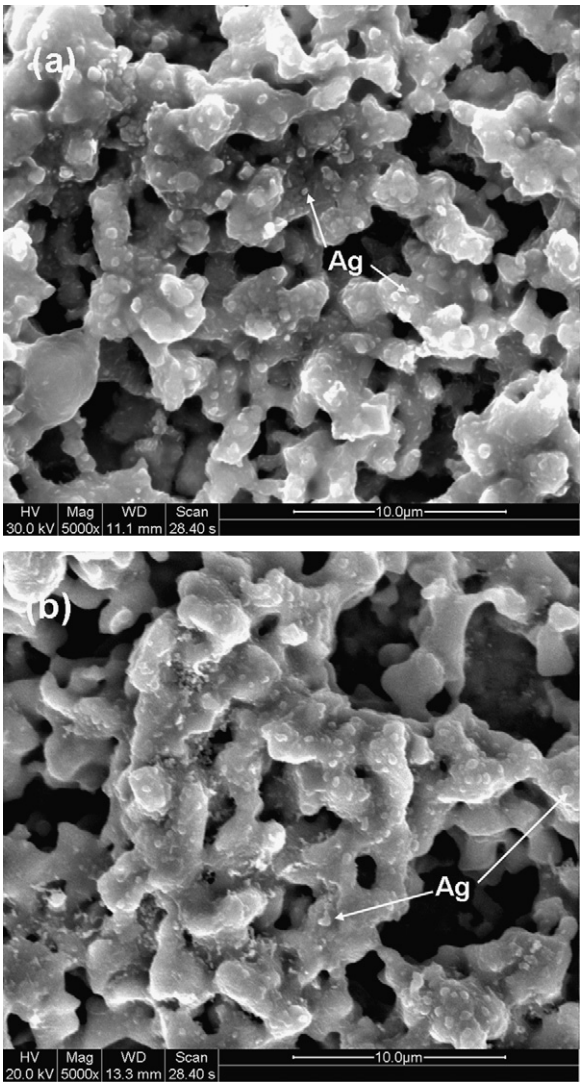

Fig. 3. SEM images of the N_2H_4-reduced Ag/BSCF (a) and HCHO-reduced Ag/BSCF (b) cathodes fired at 850 °C for 30 min.

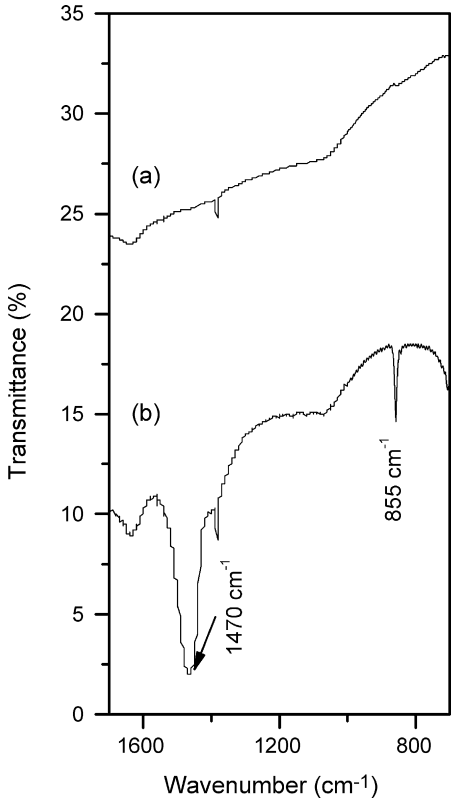

Fig. 4. FT-IR spectra of the N_2H_4-reduced Ag/BSCF (a) and HCHO-reduced Ag/BSCF (b) composite powders calcined at 900 °C.

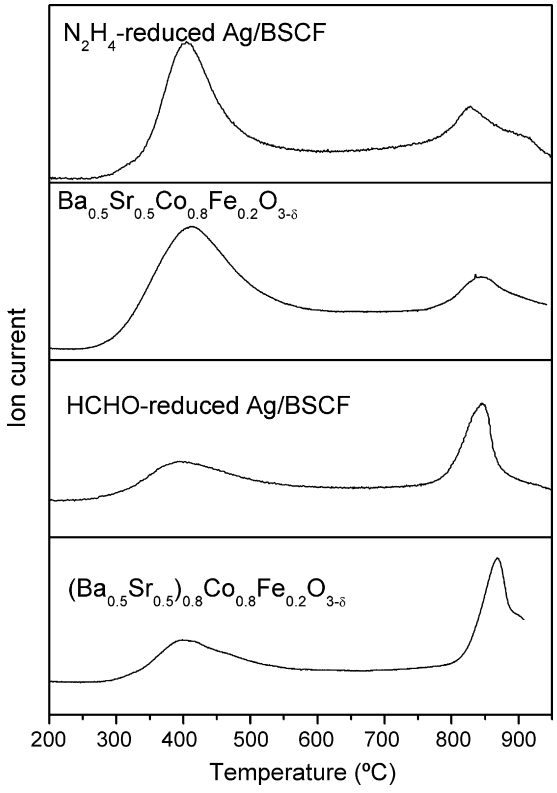

Fig. 5. . O_2-TPD curves of the N_2H_4-reduced Ag/BSCF, HCHO-reduced Ag/BSCF, pure BSCF and $(Ba_{0.5}Sr_{0.5})_{0.8}Co_{0.8}Fe_{0.2}O_{3-\delta}$.

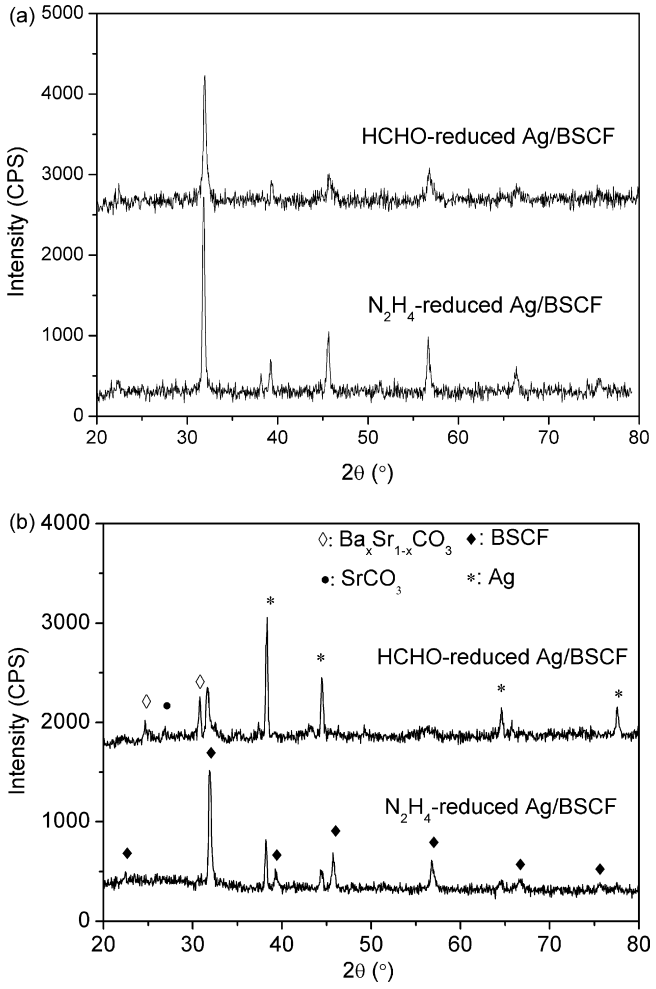

Fig. 6. XRD patterns of the Ag/BSCF composite powders calcined at 850 °C with the sliver content of 3 wt.% (a) and 30 wt.% (b).

composed of a Solartron 1260A frequency response analyzer and a Solartron 1287 potentiostat. The frequency range applied was 0.01 Hz to 100 kHz, and the signal amplitude was 10 mV under open cell voltage (OCV) conditions. The overall impedance data were fitted using a complex non-linear least squares (CNLS) fitting program from the Z-View 2.9b software.

3. Results and discussion

3.1. Morphologies and phase composition

Once the $AgNO_3$ solution was impregnated into the BSCF matrix and dried, the $AgNO_3$ was crystallized into pyramidal shape particles and dispersed uniformly over BSCF surface as shown in Fig. 1a. An aqueous solution of N_2H_4 or HCHO was then added, in drops, to the BSCF + $AgNO_3$ mixture, which was then heated to 80 °C to induce the reduction of Ag^+ to metallic Ag. Zhang et al. reported that when a Pt-Co catalyst was reduced using a 0.1 mol L^{-1} HCHO solution, aggregation was observed due to the strong reducing capability of HCHO [28]. To avoid this problem, a low concentration N_2H_4/HCHO solution at 0.01 mol L^{-1} was used in this study.

The microscopic morphologies of the as-prepared composite cathodes after the reduction are shown in Fig. 1b and c. These figures demonstrate that the Ag particles dispersed well without obvious aggregation for the Ag/BSCF electrodes prepared by both

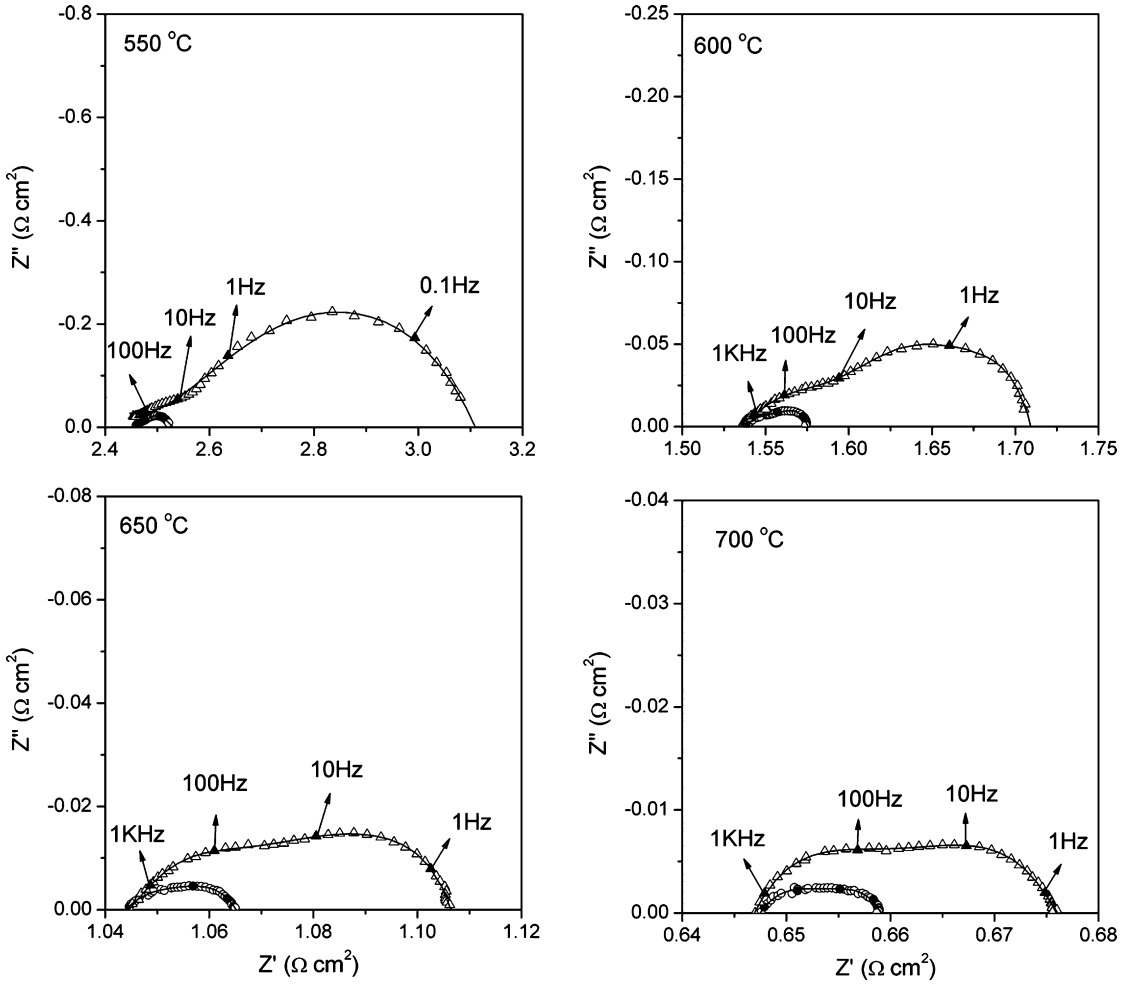

Fig. 7. Nyquist plots of the symmetrical cells with the N_2H_4-reduced Ag/BSCF (○) and HCHO-reduced Ag/BSCF (△) cathodes at 550–700 °C under open-circuit conditions.

reduction processes. However, the morphologies of the Ag particles prepared from the two different reduction processes are very different from each other. The Ag particles prepared by applying N_2H_4 as a reducing agent showed a cubic shape with a broad particle size distribution from 0.2 to 0.9 μm, while the Ag prepared via HCHO reduction showed a spherical shape with a uniform particle size of ~0.2 μm. For HCHO-reduced Ag/BSCF, besides the Ag particles, additional carbon-enriched by-products were also detected over the BSCF surface by EDX. According to Eq (4), $HCOO^-$ is released as a by-product accompanying the reduction of Ag^+ to Ag. Since $HCOO^-$ is unstable in nature, it likely reacted with the BSCF matrix to form the by-products. To learn more about the different reduction processes, the as-prepared composite powders were characterized by FT-IR. As shown in Fig. 2, the strong sharp adsorption peak at 1385 cm^{-1} was attributed to the vibration band for NO_3^-, while the peaks at 1636 and 855 cm^{-1} were attributed to the vibration bands of CO_3^{2-}. The adsorption peak for NO_3^- was very weak for the as-prepared N_2H_4-reduced Ag/BSCF, suggesting that the formed HNO_3 likely decomposed into gases. For the as-prepared HCHO-reduced Ag/BSCF, carbonate phase was detected.

In order to get rid of the organic residues and condition the silver particles, the as-prepared Ag/BSCF composites were submitted for thermal treatment. It has been reported that a firing temperature of 850 °C is optimal to get the best performance for Ag/BSCF composite cathode prepared by electroless deposition process [27]. Therefore, this temperature was used during the heat treatment of the two cathodes. Fig. 3 shows the morphologies of the two cathodes after the heat treatment at 850 °C for 30 min. The silvers in both electrodes dispersed well over the BSCF surface and took a spherical morphology with an average silver particle size of ~0.5 μm. In general, the particle size should increase after the heat treatment due to sintering. Interestingly, for the Ag in N_2H_4-reduced Ag/BSCF, the particle size reduced after the heat treatment. It was likely that the

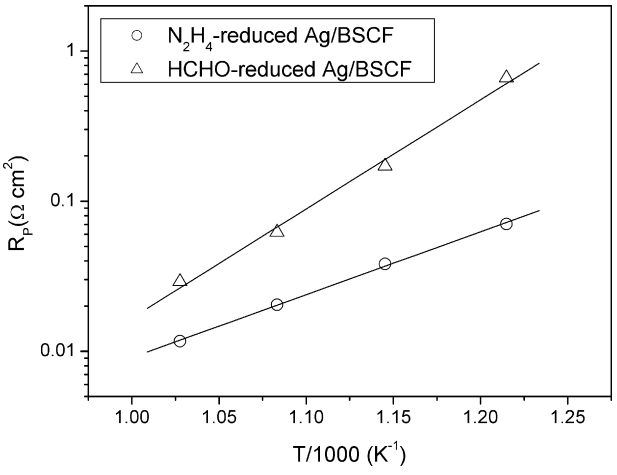

Fig. 8. Arrhenius plots of the total cathode polarization resistance (R_p) for the cells with the N_2H_4-reduced Ag/BSCF and HCHO-reduced Ag/BSCF cathodes.

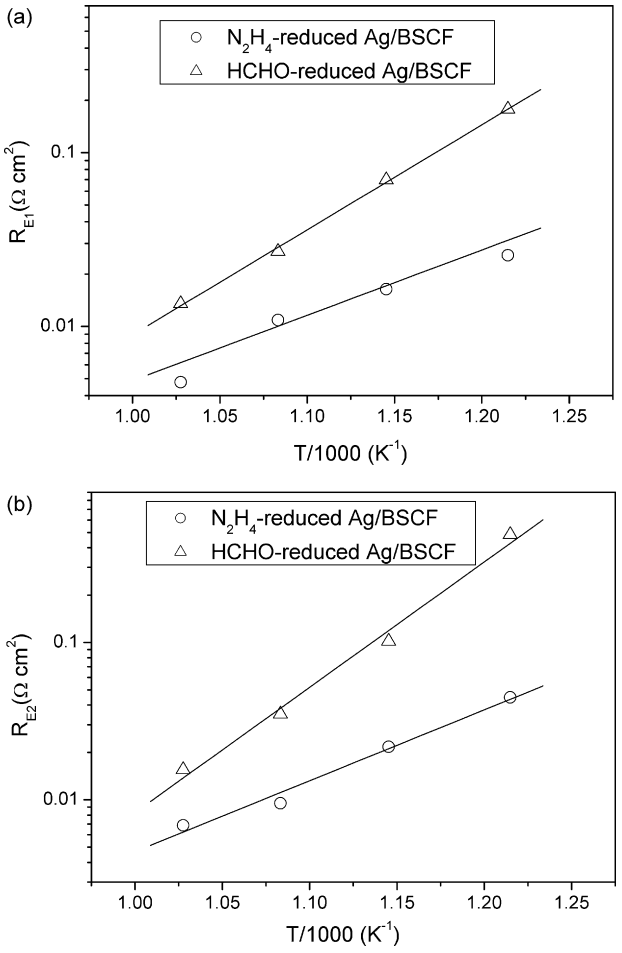

Fig. 9. Arrhenius plots of the R_{E1} (a) and R_{E2} (b) for the cells with the N_2H_4-reduced Ag/BSCF and HCHO-reduced Ag/BSCF cathodes.

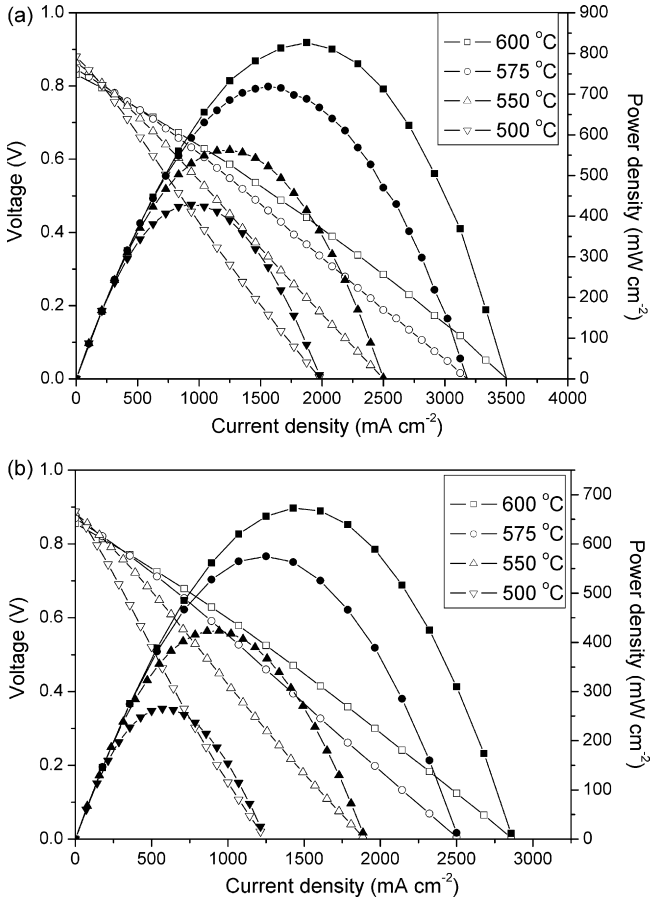

Fig. 10. *I–V* and *I–W* curves for the single cells with the N_2H_4-reduced Ag/BSCF (a) and HCHO-reduced Ag/BSCF (b) cathodes.

silver particles from the N_2H_4 reduction were in a porous structure, and thus, during the heat treatment, the particles densified, resulting in the observed shrinking.

It is well known that the formation of carbonate over the perovskite surface can block oxygen surface diffusion and thereby reduce the electrochemical activity of the oxide for ORR. In order to get rid of such surface carbonates, thermal decomposition is usually applied. Due to the high sintering capability and low melting point of silver, a firing temperature lower than 900 °C should be employed [27]. The FT-IR spectra of the Ag/BSCF composites after firing at 900 °C are shown in Fig. 4. The vibration band for NO_3^- vanished after the heat treatment. However, the vibration band for CO_3^{2-} was still observed in HCHO-reduced Ag/BSCF electrode. This implies that such a thermal treatment temperature is insufficient to remove the surface carbonate. It has also been reported that carbonates can only be eliminated thoroughly at temperature higher than 950 °C under an argon atmosphere [29]. However, such a high temperature would result in sintering or melting of the silver.

Temperature-programmed oxygen desorption (O_2-TPD) curves of the Ag/BSCF composites prepared from the two different reduction processes and fired at 850 °C are depicted in Fig. 5. Oxygen desorption occurred in two separate zones, which started at approximately 300 and 800 °C, respectively. For convenience, the oxygen desorbed in these two zones is labeled α- and β-oxygen, respectively [32]. The O_2-TPD reflects the change of oxidation states of cobalt and iron in BSCF. The oxygen desorption at the lower temperature zone, i.e., α-oxygen, is associated with the reduction of Co^{4+}/Fe^{4+} to Co^{3+}/Fe^{3+}, while the β-oxygen desorption process is associated with the reduction of Co^{3+} to Co^{2+}. The oxygen desorption characteristic for N_2H_4-reduced Ag/BSCF is similar to pure BSCF. This implies the micro-structure and phase composition of the BSCF using N_2H_4 as the reducing agent was not altered significantly. For the case of HCHO-reduced Ag/BSCF, the

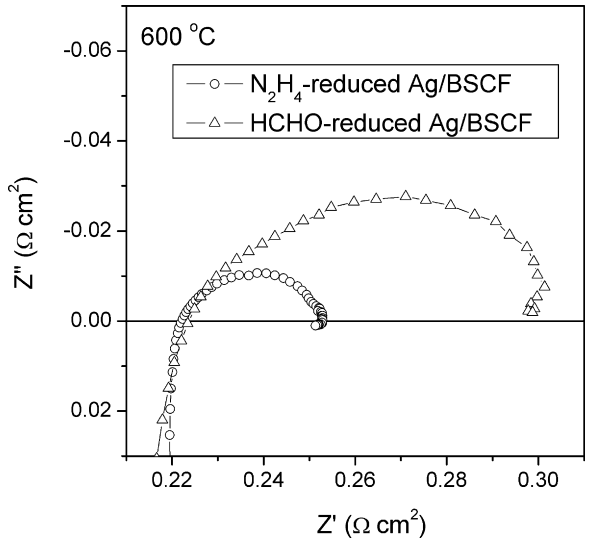

Fig. 11. AC impedance spectra for the single cells with the two composite cathodes measured at 600 °C under open circuit conditions.

intensity of the α-oxygen decreased while the intensity of β-oxygen increased. The A-site cation-deficient BSCF, with a composition of $(Ba_{0.5}Sr_{0.5})_{0.8}Co_{0.8}Fe_{0.2}O_{3-\delta}$, was also tested for comparison. The profiles for HCHO-reduced Ag/BSCF and the A-site deficient BSCF are very similar, which indicates the possible formation of an A-site cation deficient BSCF in the HCHO-reduced Ag/BSCF electrode. This agrees well with the fact that the HCOOH has a relatively high acidity and it is prone to react with Ba or Sr in BSCF. Consequently, some of the Ba and Sr were lost in BSCF, which lead to formation of the A-site deficient BSCF. Due to the low concentration of Ag (3 wt.%) and by-products in Ag/BSCF composite, they can not be detected by XRD as shown in Fig. 6a. In order to further verify above results, the ratio of $AgNO_3$/BSCF was increased to 30 wt.%. XRD patterns of the Ag/BSCF composite powders calcined at 850 °C are shown in Fig. 6b. The diffraction peaks of the N_2H_4-reduced Ag/BSCF composite powders can still be indexed well to BSCF and Ag. This implies that the N_2H_4 successfully reduced Ag^+ to Ag without damaging the BSCF phase, even at a much higher dosage. However, for the HCHO-reduced Ag/BSCF composite, the carbonates in the family of $Ba_xSr_{1-x}CO_3$ were detected as well as the BSCF and Ag main phases.

3.2. Electrochemical behavior

Nyquist plots of the symmetrical cells were obtained at 550–700 °C under open-circuit conditions. As shown in Fig. 7, all impedance spectra contain two separable depressed arcs, suggesting that at least two different electrode processes limited the oxygen reduction reaction. In order to separate these two processes, the impedance spectra were fitted to an equivalent circuit with a standardized configuration of $R_{ohm}(R_{E1}-CPE_1)(R_{E2}-CPE_2)$. The overall ohmic resistance, R_{ohm}, includes the electrolyte resistance, the electrode ohmic resistance, and the lead resistance. The high-frequency resistance is probably associated with charge-transfer processes (R_{E1}). The low-frequency arc is ascribed to diffusion processes (R_{E2}), including the adsorption–desorption of oxygen, oxygen diffusion at the gas-cathode interface, and the surface diffusion of intermediate oxygen species [27,33–40]. The difference between the real axes intercepts of the impedance plot is considered to be the cathode polarization resistance ($R_p = R_{E1} + R_{E2}$). The symbols in Fig. 7 represent the measured data, and the solid lines are fitted curves. Good agreement is observed between the equivalent circuit and the observed impedance data. This implies that the equivalent circuit is a reasonable approximation. As can be seen, the preparation methods evidently influenced both the charge-transfer and diffusion processes. The cell with the N_2H_4-reduced Ag/BSCF cathode showed smaller arcs at all operating temperatures.

Fig. 8 shows the Arrhenius plots of the total cathode polarization resistance (R_p) for the cells with the cathodes prepared by the two different methods. Some studies have shown that adding Ag to the BSCF matrix improved the electrochemical performance of the electrode [26,27]. A similar trend was also observed for the N_2H_4-reduced Ag/BSCF cathode in this study. For example, the value of R_p is only 0.038 Ω cm^2 at 600 °C, lower than the value of pure BSCF reported by our previous studies [32,41]. However, the values of R_p for the HCHO-reduced Ag/BSCF cathode are much higher than those of the pure BSCF. The apparent activation energies of the oxygen reduction reaction obtained from the slopes of the plots in Fig. 8 are listed in Table 1. The activation energy of the R_p is 80.1 kJ mol^{-1} for the N_2H_4-reduced Ag/BSCF, which is lower than the value of ~109 kJ mol^{-1} for the pure BSCF [32], while the activation energy of R_p for the HCHO-reduced Ag/BSCF is as high as 138.9 kJ mol^{-1}.

The fitted impedance parameters are given in Fig. 9. For the pure BSCF cathode, the resistances are 0.044 and 0.063 Ω cm^2 for the charge-transfer process and the diffusion process at 600 °C, respectively [32]. As compared to pure BSCF electrode, these two processes were improved for the N_2H_4-reduced Ag/BSCF cathode, while the two processes deteriorated for the HCHO-reduced Ag/BSCF cathode. The carbonates in the HCHO-reduced Ag/BSCF cathode not only blocked the oxygen adsorption and surface diffusion, but also occupied the active sites for oxygen reduction. Therefore, an increase of the R_{E1} and R_{E2}, and thus an increase in the activation energies for these two processes, was observed for the HCHO-reduced Ag/BSCF (Table 1).

Table 1
Activation energies of R_{E1}, R_{E2} and R_p for the N_2H_4-reduced Ag/BSCF and HCHO-reduced Ag/BSCF cathodes.

Cathodes	Activation energy (kJ mol^{-1})		
	R_{E1}	R_{E2}	R_p
N_2H_4-reduced Ag/BSCF	71.9	86.2	80.1
HCHO-reduced Ag/BSCF	115.6	152.3	138.9

3.3. Single-cell performance

Complete fuel cells adopting the HCHO-reduced Ag/BSCF and N_2H_4-reduced Ag/BSCF cathodes were built based on the thin-film SDC electrolyte. Fig. 10 shows the performances of the single cells using H_2 as the fuel and air as the cathode atmosphere, operated at 500–600 °C. A peak power density of 826 mW cm^{-2} was achieved for the cells with the N_2H_4-reduced Ag/BSCF cathode at 600 °C. As expected, poorer performances were observed for the cells based on the HCHO-reduced Ag/BSCF cathodes. The peak power density at 600 °C was only 672 mW cm^{-2} for the cell with the HCHO-reduced Ag/BSCF cathode. Shown in Fig. 11 are the typical impedance spectra for the cells with the two composite cathodes, measured at 600 °C under open circuit conditions. Here, the intercept with the real axis at high frequencies represents the resistance of the electrolyte and lead wires (about 0.22 Ω cm^2), whereas the resistance between the two intercepts with the real axis corresponds to the impedance of the two interfaces, i.e. the cathode-electrolyte interface and the anode-electrolyte interface. The electrode ASRs are 0.048 and 0.079 Ω cm^2 for the cells with the N_2H_4-reduced Ag/BSCF and HCHO-reduced Ag/BSCF cathodes, respectively. Since the anodes are identical, the differences in the electrode ASRs can be essentially attributed to the cathode. Our previous studies also indicated that the carbonates in the cathode can significantly influence the ORR activity, and eliminating the carbonates is helpful to improve the cathode performance [29,30].

4. Conclusions

The Ag/BSCF composite cathodes for LT-SOFCs were prepared by electroless deposition using N_2H_4 and HCHO as reducing agents. The silver particles originating from the two processes have similar particle sizes and dispersion over the BSCF surface. As compared to a pristine BSCF electrode, the electrochemical performance of the composite cathode was improved by using N_2H_4 as the reducing agent. The ASR of N_2H_4-reduced Ag/BSCF was as low as 0.038 Ω cm^2 at 600 °C. However, when the HCHO was used as the reducing agent, the carbonates in the family of $Ba_xSr_{1-x}CO_3$ formed during the preparation, which blocked the active sites for oxygen adsorption and reduction reactions and led to an increase in the polarization resistances of both the charge-transfer process and the diffusion process. As a result, the anode-supported single cell with the N_2H_4-reduced Ag/BSCF cathode showed improved performance and reached peak power densities of 826, 562 and 428 mW cm^{-2} at 600, 550 and 500 °C, respectively. Reducing agents that could lead to the formation of carbonates are not recommended in the

preparation of silver-modified perovskite electrode that contained Ba and/or Sr alkaline earth metal ions.

Acknowledgements

This work was supported by the National Natural Science Foundation of China under contract Nos. 20703024, and 20676061, by the National 863 program under contract No. 2007AA05Z133, and by the National Basic Research Program of China under contract No. 2007CB209704.

References

[1] B.C.H. Steele, A. Heinzel, Nature 414 (2001) 345–352.
[2] M.J.L. Ostergard, C. Clausen, C. Bagger, M. Mogensen, Electrochim. Acta 40 (1994) 1971–1981.
[3] D. Hirabayashi, A. Tomita, S. Teranishi, T. Hibino, M. Sano, Solid State Ionics 176 (2005) 881–887.
[4] T. Hibino, A. Hashimoto, T. Inoue, J. Tokuno, S. Yoshida, M. Sano, Science 288 (2000) 2031–2033.
[5] E.P. Murray, S.A. Barnett, Solid State Ionics 143 (2001) 265–273.
[6] Z.P. Shao, S.M. Haile, Nature 431 (2004) 170–173.
[7] Z.P. Shao, S.M. Haile, J. Ahn, P.D. Ronney, Z. Zhan, S.A. Barnett, Nature 435 (2005) 795–798.
[8] F.L. Liang, J. Chen, J.L. Cheng, S.P. Jiang, T.M. He, J. Pu, J. Li, Electrochem. Comm. 10 (2008) 42–46.
[9] T. Kenjo, S. Osawa, K. Fujikawa, J. Electrochem. Soc. 138 (1991) 349–355.
[10] S.P. Simner, M.D. Anderson, J.W. Templeton, J.W. Stevenson, J. Power Sources 168 (2007) 236–239.
[11] R. Baker, J. Guindet, M. Kleitz, J. Electrochem. Soc. 144 (1997) 2427–2432.
[12] M. Sahibzada, S.J. Benson, R.A. Rudkin, J.A. Kilner, Solid State Ionics 113–115 (1998) 285–290.
[13] K. Sasaki, J. Tamura, M. Dokiya, Solid State Ionics 144 (2001) 233–240.
[14] S.P. Simner, M.D. Anderson, J.E. Coleman, J.W. Stevenson, J. Power Sources 161 (2006) 115–122.
[15] M. Watanabe, H. Uchida, M. Shibata, N. Mochizuki, K. Amikura, J. Electrochem. Soc. 141 (1994) 342–346.
[16] K. Sasaki, K. Hosoda, T.N. Lan, K. Yasumoto, S. Wang, M. Dokiya, Solid State Ionics 174 (2004) 97–102.
[17] L.S. Wang, S.A. Barnett, Solid State Ionics 76 (1995) 103–113.
[18] J.D. Zhang, Y. Ji, H.B. Gao, T.M. He, J. Liu, J. Alloys Compd. 395 (2005) 322–325.
[19] T.Z. Sholklapper, V. Radmilovic, C.P. Jacobson, S.J. Visco, L.C. De Jonghe, J. Power Sources 175 (2008) 206–210.
[20] W. Zhou, Z.P. Shao, R. Ran, Z.H. Chen, P.Y. Zeng, H.X. Gu, W.Q. Jin, N.P. Xu, Electrochim. Acta 52 (2007) 6297–6303.
[21] V.A.C. Haanappel, D. Rutenbeck, A. Mai, S. Uhlendruck, D. Sebold, H. Wesemeyer, B. Rowekamp, C. Tropartz, F. Tietz, J. Power Sources 130 (2004) 119–128.
[22] Y. Liu, M. Mori, Y. Funahashi, Y. Fujishiro, A. Hirano, Electrochem. Comm. 9 (2007) 1918–1923.
[23] S.R. Wang, T. Kato, S. Nagata, T. Honda, T. Kaneko, N. Iwashita, M. Dokiya, Solid State Ionics 146 (2002) 203–210.
[24] Y. Sakito, A. Hirano, N. Imanishi, Y. Takeda, O. Yamamoto, Y. Liu, J. Power Sources 182 (2008) 476–481.
[25] S.H. Huang, Z.Y. Wen, J.C. Zhang, X.L. Yang, Electrochim. Acta 52 (2007) 3704–3708.
[26] R. Su, Z. Lü, K.F. Chen, N. Ai, S.Y. Li, B. Wei, W.H. Su, Electrochem. Commun. 10 (2008) 844–847.
[27] W. Zhou, R. Ran, Z.P. Shao, R. Cai, W.Q. Jin, N.P. Xu, J. Ahn, Electrochim. Acta 53 (2008) 4370–4380.
[28] L. Zhang, K.C. Lee, J.J. Zhang, Electrochim. Acta 52 (2007) 7964–7971.
[29] W. Zhou, Z.P. Shao, R. Ran, H.X. Gu, W.Q. Jin, N.P. Xu, J. Am. Ceram. Soc. 91 (2008) 1155–1162.
[30] W. Zhou, R. Ran, Z.P. Shao, W. Zhuang, J. Jia, H.X. Gu, W.Q. Jin, N.P. Xu, Acta Mater. 56 (2008) 2687–2698.
[31] W. Zhou, Z.P. Shao, W.Q. Jin, J. Alloys Compd. 426 (2006) 368–374.
[32] W. Zhou, R. Ran, Z.P. Shao, W.Q. Jin, N.P. Xu, J. Power Sources 182 (2008) 24–31.
[33] S.B. Adler, J.A. Lane, B.C.H. Steele, J. Electrochem. Soc. 143 (1996), 3554-2564.
[34] X.J. Chen, S.H. Chan, K.A. Khor, Electrochim. Acta 49 (2004) 1851–1861.
[35] F. Qiang, K.N. Sun, N.Q. Zhang, X.D. Zhu, S.R. Le, D.R. Zhou, J. Power Sources 168 (2007) 338–345.
[36] S.B. Adler, Solid State Ionics 111 (1998) 125–134.
[37] M.J. Jørgensen, M. Mogensen, J. Electrochem. Soc. 148 (2001) A433–A442.
[38] S.P. Jiang, W. Wang, J. Electrochem. Soc. 152 (2005) A1398–A1408.
[39] M. Koyama, C. Wen, T. Masuyama, J. Otomo, H. Fukunaga, K. Yamada, K. Eguchi, H. Takahashi, J. Electrochem. Soc. 148 (2001) A795–A801.
[40] M.J. Escudero, A. Aguadero, J.A. Alonso, L. Daza, J. Electroanal. Chem. 611 (2007) 107–116.
[41] W. Zhou, R. Ran, Z.P. Shao, H.X. Gu, W.Q. Jin, N.P. Xu, J. Power Sources 174 (2007) 237–245.